crystals

MDPI

Article

Calculated Outstanding Energy-Storage Media by Aluminum-Decorated Carbon Nitride (g-C_3N_4): Elucidating the Synergistic Effects of Electronic Structure Tuning and Localized Electron Redistribution

Peng Gao [1,2], Zonghang Liu [3,*], Jiefeng Diao [4], Jiaao Wang [4,5,*], Jiwen Li [6], Yuebin Tan [7], Guangtong Hai [8] and Graeme Henkelman [4,*]

1 School of Chemistry and Molecular Bioscience, University of Wollongong, Northfields Avenue, Wollongong, NSW 2500, Australia
2 Molecular Horizons, University of Wollongong, Wollongong, NSW 2500, Australia
3 School of Chemistry and Chemical Engineering, University of Jinan, Jinan 250022, China
4 Department of Chemistry and the Oden Institute for Computational Engineering and Sciences, The University of Texas at Austin, 105 E. 24TH ST. STOP A5300, Austin, TX 78712, USA
5 AI for Science Group, Bytedance Inc., 151 W 42nd Street, New York, NY 10036, USA
6 College of Physics and Electronic Engineering, Northwest Normal University, Lanzhou 730070, China
7 Department of Biochemistry and Molecular & Cellular Biology, Georgetown University, Washington, DC 20007, USA
8 Beijing Key Laboratory of Membrane Materials and Engineering, Department of Chemical Engineering, Tsinghua University, Beijing 100084, China
* Correspondence: liuzonghang@cuhk.edu.cn (Z.L.); wangjiaao0720@utexas.edu (J.W.); henkelman@utexas.edu (G.H.)

check for updates

Citation: Gao, P.; Liu, Z.; Diao, J.; Wang, J.; Li, J.; Tan, Y.; Hai, G.; Henkelman, G. Calculated Outstanding Energy-Storage Media by Aluminum-Decorated Carbon Nitride (g-C_3N_4): Elucidating the Synergistic Effects of Electronic Structure Tuning and Localized Electron Redistribution. *Crystals* **2023**, *13*, 655. https://doi.org/10.3390/cryst13040655

Academic Editors: Maija Nissinen, Xingfang Liu and Rubi Gul

Received: 13 January 2023
Revised: 17 March 2023
Accepted: 20 March 2023
Published: 11 April 2023

Abstract: Hydrogen, as an important clean energy source, is difficult to store and transport, which hinders its applications in real practice. Developing robust yet affordable storage media remains to be a challenge for scientists. In this study, Ab Initio Molecular Dynamics (AIMD) simulations were employed to evaluate the performance of aluminum (Al) decorated carbon nitride (g-C_3N_4, heptazine structure) in hydrogen storage; and a benchmarking study with Mg-doped g-C_3N_4 was also performed to provide theoretical insights for future study. We found that each 2 × 2 supercell can accommodate four Al atoms, and that partial charge from single Al sites can be transferred to adjacent nitrogen atoms of g-C_3N_4. These isolated Al sites tend to be electronically positive charged, serving as active sites for H_2 adsorption, predominately by triggering enhanced electrostatic interactions. The H_2 molecules are adsorbed by both Al and N atoms, and are easily polarized, giving rise to electrostatic interactions between the gas molecules and the surface. Effective adsorption sites were determined by electronic potential distribution maps of the optimized configurations. Each 2 × 2 supercell can adsorb up to 36 H_2 molecules, and the corresponding adsorption energies are within the range of −0.10 to −0.26 eV. The H_2 storage capacity of the Al-decorated g-C_3N_4 is 7.86 wt%, which surpasses the goal of 5.5 wt%, set by the US department of energy. This proposed Al-decorated g-C_3N_4 material is therefore predicted to be efficient for hydrogen storage. This work may offer some fundamental understandings from the aspect of electronic sharing paradigm of the origin of the excellent hydrogen storage performance by metal decorated 2D materials, acting as an demonstration for guiding single metal atom site-based materials' designing and synthesis.

Keywords: DFT; hydrogen capture; two-dimensional materials; C_3N_4; energy materials

1. Introduction

In the context of the global energy crisis and high CO_2 emissions, finding alternative sources of renewable energy is becoming increasingly important. Hydrogen has long been envisioned as the fuel of future, due to its potential low environmental impact [1].

Hydrogen fuel-cell powered vehicles, for example, have zero-emission if the hydrogen is produced from renewable energy [2,3]. Unfortunately, in practice, the utilization of hydrogen as an energy carrier is challenging with the most significant hurdles being associated with its storage and delivery [4,5]. Traditional hydrogen storage requires high-pressures of 700 bar, leading to possible safety issues, so the development of materials-based hydrogen storage media is an important goal. Over the past decades, various kinds of materials have been used for hydrogen storage, including metal hydrides [6–9], liquid hydrocarbons [10], boron-containing compounds [11–16], etc. The ideal candidates should be competitive in terms of both synthetic convenience and adsorption capacity, as compared to high pressure cells, rather than just favoring one attribute over the other.

In recent years, two dimensional (2D) graphitic carbon nitrides with porous structures were found to have many attractive properties for various kinds of applications [17–27]. Among them, g-C_3N_4, which was first proposed by Liu et al. [28], has structural hardness, and based on its porous structure, materials with desirable adsorption properties can be decorated on its surface [29–38]. Additionally, a number of metals were found to bind with C/N atoms in g-C_3N_4, and the binding energies of adsorbates were found to be in a useful range. For example, Ruan et al. found that within a 2 × 2 supercell of g-C_3N_4, the adsorption energy of single Li atom at each pore is close to −2.11 eV. Zhang et al. also found that the structure of g-C_3N_4 is suitable for the well-dispersed decoration of transition metals including Sc, Ti as well as Li [32]. However, the binding mechanism still remains to be theoretically elucidated. It is also notable that with the decoration of active metals, the g-C_3N_4 was modified to be suitable for gas adsorption [35]. Nair et al. investigated the H_2 storage performance of Pd-decorated g-C_3N_4, and the capacity of adsorption was found to reach 2.6 wt% [30]. Zhu et al. evaluated the performance of Li decorated g-C_3N_4 and reported an adsorption energy per H_2 of −0.15 eV with a corresponding 4.5 wt% capacity [29]. It has been found that each metal atom can usually adsorb multiple gas molecules, for instance, Wu et al. determined that each Li atom interacts with up to three H_2 molecules [33]. Presently, there remain two important factors that need to be understood to further improve the design of hydrogen-storage materials: (i) the precise binding motif between the decoration metals and C/N atoms from g-C_3N_4; and (ii) a correlation between the electronic structure of the metal-decorated g-C_3N_4 and performance for gas adsorption.

In this paper, we focused on Al-decorated g-C_3N_4; and to provide theoretical insights of metal binding within this class of 2D materials for future study, a benchmarking study with Mg-decorated g-C_3N_4 was conducted. We first applied density functional theory (DFT) calculations to obtain its optimized structure, and then summarized the factors that may determine its performance for H_2 adsorption. The migration of an Al atom within the pore of g-C_3N_4 was energetically investigated; and the hydrogen storage configurations were also presented for reference. We anticipate that the findings provided in this study will assist the development of novel 2D materials that are suitable for clean energy gas storage.

2. Computational Details

DFT calculations were carried out with the Vienna Ab-initio Simulation Package (VASP) [39,40]. The lattice parameters of the g-C_3N_4 supercell were set to a = 14.26 Å and b = 14.26 Å. The generalized gradient approximation in the form proposed by Perdew-Burke-Ernzerh of [41,42] was applied to calculate the exchange-correlation energies. The electronic states were expanded in a plane wave basis with an energy cutoff of 520 eV. The core-valence interactions were described by the projector augmented wave method [43]. Van der Waals corrections were described with the DFT-D2 method [40]. The Al-decorated g-C_3N_4 system contained 60 atoms; for the 2 × 2 supercell a Gamma-centered k-point grid of 3 × 3 × 1 was used to sample the Brillouin zone [44,45]. A vacuum layer of 30 Å was used to isolate the periodic slabs in the c direction. Structural relaxations were done with the conjugate-gradient algorithm. The convergence criterion of the Hellmann-Feynman forces was set to 0.05 eV/Å and 10^{-5} eV for the electronic structure. All the computational parameters were verified to be acceptable in terms of calculation accuracy and resource cost.

Band gap calculations were performed with the Heyd–Scuseria–Ernzerhof (HSE06) hybrid functional [46]. The charge transfer between the metal atoms and the g-C_3N_4 surface were evaluated with a Bader charge analysis [47].

For Al atoms on the pristine g-C_3N_4, the adsorption energy was obtained by

$$E_{ads}(Al) = [E(Al_n \circ C24N32) - E(C24N32) - nE(Al)]/n(Al), \quad (1)$$

where n(Al) is the number of Al atoms, and E is the energy. The adsorption energy per hydrogen molecule was calculated as

$$E_{ads}(H2) = [E(kH2 \bullet Al_n \circ C24N32) - E(Al_n \circ C24N32) - kE(H2)]/m(H2), \quad (2)$$

where k(H_2) is the number of hydrogen molecules that are adsorbed on the Al-decorated g-C_3N_4 surface.

To explore conditions of H_2 desorption from the Al-decorated g-C_3N_4, the desorption temperature, T_D, was calculated with the van't Hoff equation

$$T_D = \frac{E_{ads}}{k_b}\left(\frac{\Delta S}{R} - \ln P\right)^{-1} \quad (3)$$

where k_b and R are the Boltzmann constant and universal gas constant, respectively; ΔS is the change of H_2 entropy from the gas to liquid state (75.44 J mol^{-1} K^{-1}); P is the pressure (1 atm).

3. Results and Discussion

3.1. Structural Properties and Al Binding

Al adsorption sites on g-C_3N_4 both close to the C/N atom or slightly above the pores were considered. Favorable adsorption is found close to N atoms where the adsorbed Al atom binds to two neighboring N atoms with an adsorption energy of −3.42 eV, as shown in Figure 1. Such a value is comparable to that of Mg-decorated g-C_3N_4 [37]; and the behind reason may lie in the fact that the valence electrons distributions for these two metals are different to each other. The binding between the adsorbed Al and the two neighboring N atoms is associated with charge transfer, as discussed in the following section. The structure of the Al-decorated g-C_3N_4 is somewhat twisted so that the Al are slightly out of the plane. In this study, we focus on a single Al atom adsorption within the pore of g-C_3N_4; the reason behind this lies in the fact that placement of multiple large metal atoms in the same pore may hinder gas molecules adsorption. Based on previous studies, for metal atoms with a smaller size, including Li, multiple adsorbed atoms at the same pore may still facilitate gas adsorption [48].

From the computed density of states (DOS), we found that the conductivity of Al-decorated g-C_3N_4 was improved, confirming the binding and charge transfer between the Al and N atoms. In Figure 2, the partial density of states (PDOS) were plotted for the 2p orbitals of N and C atoms, showing that these two orbitals are hybridized. With the decoration of Al, mid-band states were found to appear at the Fermi level, as shown in Figure 3. The strong overlap between the 3p/3s orbitals of Al and the hybrid orbitals of C/N further demonstrate the chemical interactions between Al and the surface. Our ELF calculation (Figure 4) shows that there exists chemical interaction between Al and N atoms. It is possible that the 3p/3s electrons from Al are first hybridized, and then the Al can bind with its neighboring N atoms. Thus, we can confirm that the overall electronic structure of the metal-decorated g-C_3N_4 is largely dependent on the electronic structure of the deposited metal atoms. To more clearly determine the binding interaction between Al and the g-C_3N_4, a Bader analysis was conducted to estimate the amount of charge transfer, which is 1.2 e^- from Al to the g-C_3N_4. The charge density difference for Al-decorated g-C_3N_4 is shown in Figure 5. The higher electronegativity of C/N enables electron gain from Al. By comparison, the Al atom's capacity of electron donating is weaker than that of

Mg atom within the pore of g-C_3N_4 (1.6 e^-); and this explains why the adsorption of Al is relatively weaker [37]. Additionally, we found that in the bound structure, Al was polarized to form a local electronic field with some regions having considerable electropositivity. In addition, the deposition of Al also successfully transformed the semiconducting g-C_3N_4 monolayer into a conductor as shown in Figure 6. It is likely that the electronic structure of the metal-decorated g-C_3N_4 largely determines its H_2 adsorption properties.

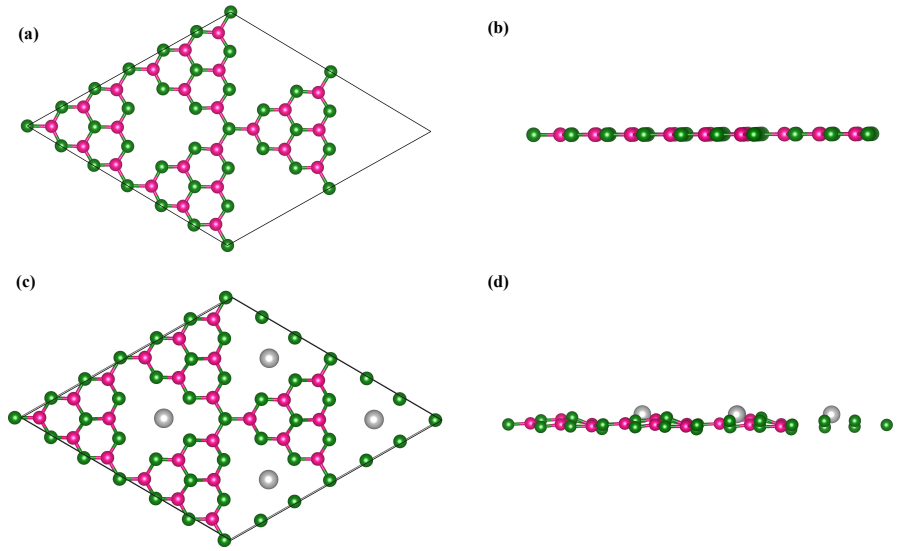

Figure 1. Optimized configurations of the g-C_3N_4 monolayer (**a**,**b**) and the Al-decorated g-C_3N_4 (**c**,**d**). Green, pink, and silver spheres represent N, C and Al atoms, respectively.

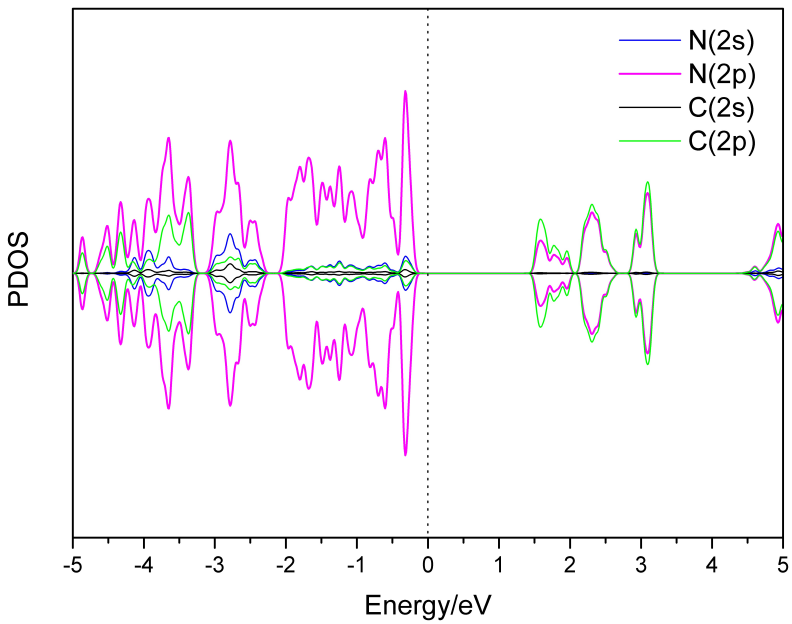

Figure 2. The partial density of states (PDOS) of the g-C_3N_4 monolayer for selected N and C atoms. The energy was plotted with respect to the Fermi energy.

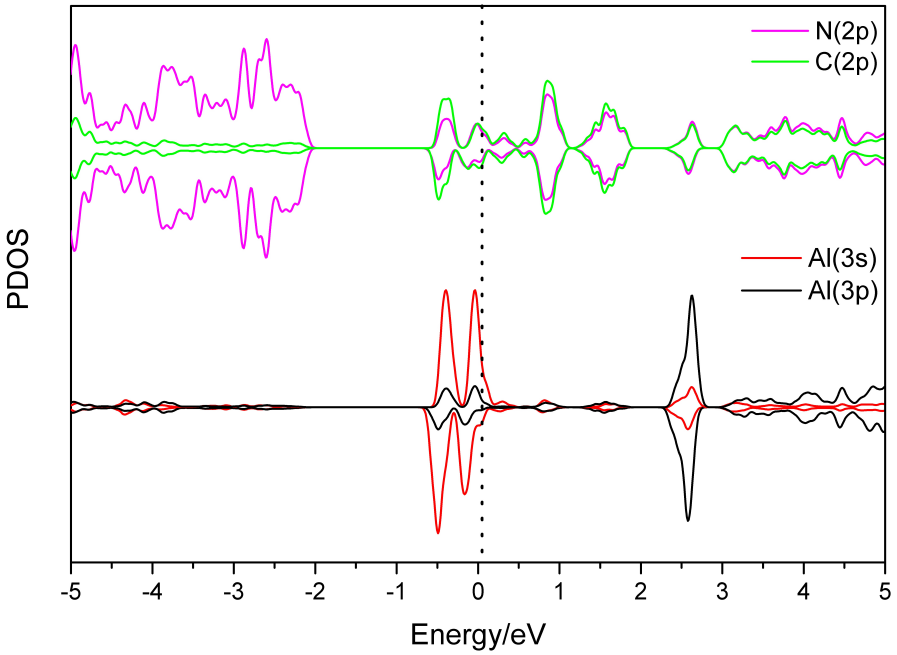

Figure 3. The PDOS of the Al-decorated g-C_3N_4 for selected N, C and Al atoms. The energy is plotted with respect to the Fermi energy.

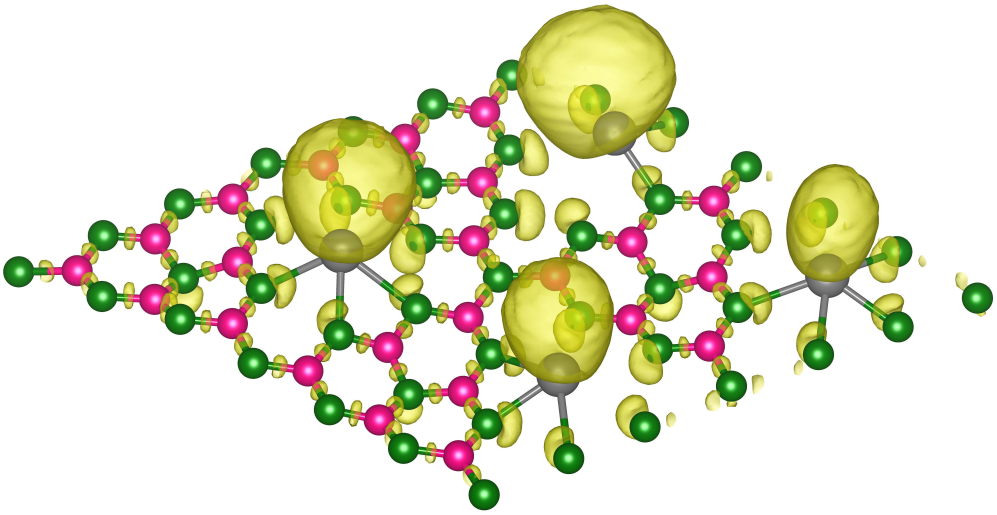

Figure 4. The calculated electron localization function (ELF) of Al-decorated g-C_3N_4; the isosurface around Al and N atoms corresponds to an ELF value of 0.7.

To test the stability of the Al-decorated g-C_3N_4, DFT molecular dynamics (MD) simulations were performed. As shown in Figure 7, the system is heated from 10 K to 1200 K during a period of 8 ps and then simulated for another 10 ps. We can see that the overall structure of this composite material is stable until the temperature is increased to 700 K, at least on the accessible MD time scales. However, once the system is overheated, the Al atoms tend to desorb from the g-C_3N_4 monolayer.

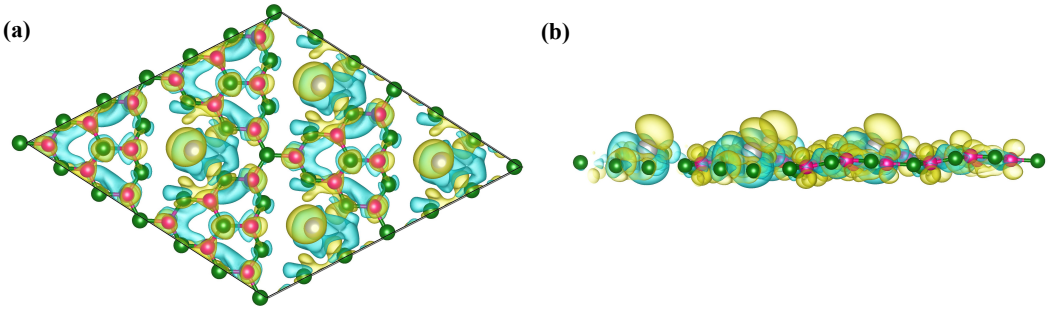

Figure 5. Charge density difference for the Al-decorated g-C_3N_4, (**a**) top and (**b**) side view. Yellow regions indicate charge gain and the blue regions indicates charge loss. The isosurface of charge density is 0.003 e/Bohr^3.

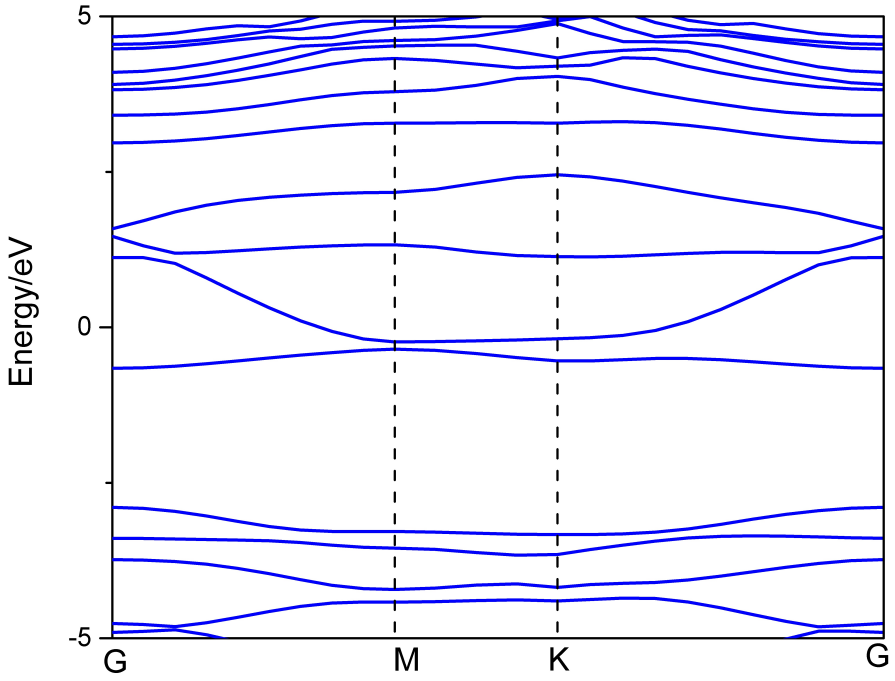

Figure 6. Band structure of the Al−decorated g−C_3N_4 calculated with the HSE06 functional.

To further measure the difficulty of Al atom's migration among the surface of g-C_3N_4, the Adaptive Kinetic Monte Carlo (AKMC) [49–51] method was applied. We found that the pore migration barrier for single Al atom is around 0.634 eV (more details can be seen in Figure 8), and the barrier for Al to escape the pore is larger than 2 eV. These calculation results indicate that the proposed configuration of Al-decorated g-C_3N_4 is chemically stable. Moreover, a systematic benchmarking study with Mg-decorated g-C_3N_4 was also conducted for reference; and we noticed that for Mg atoms, the corresponding energy barrier is even larger, indicating that the migration of Mg atoms upon the surface of g-C_3N_4 is more difficult than that of Al atoms. The two metal atoms own different electronic structures. These observations are consistent with our previous studies, further demonstrating that this kind of 2D materials are applicable in real practice [37].

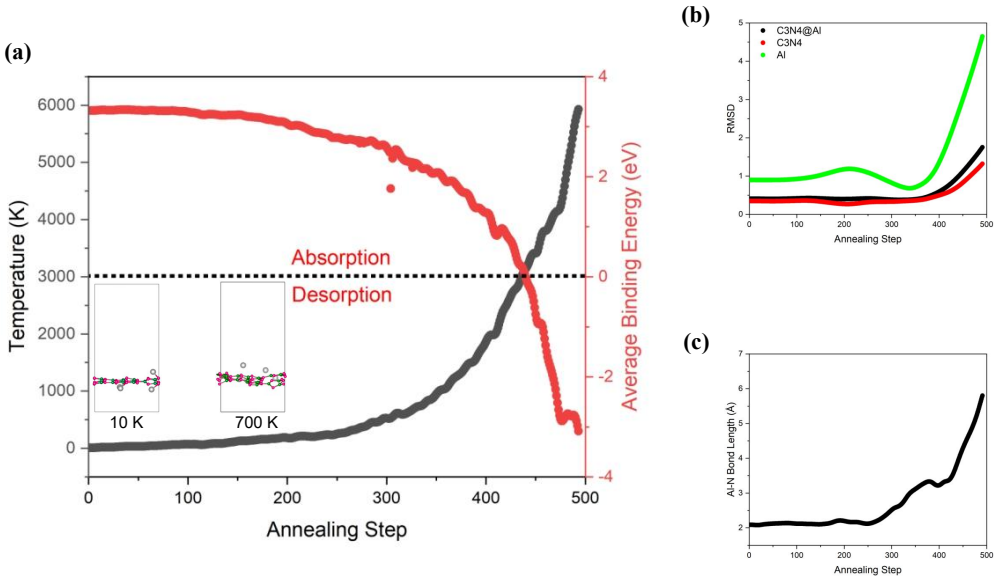

Figure 7. DFT MD simulations of the Al−decorated g-C_3N_4, (**a**) adsorption/desorption process, (**b**) RMSD (root mean square deviation) and (**c**) the change of Al-N bond length. The system is heated from 10 K to 1200 K, and the time step is set to 1.0 fs.

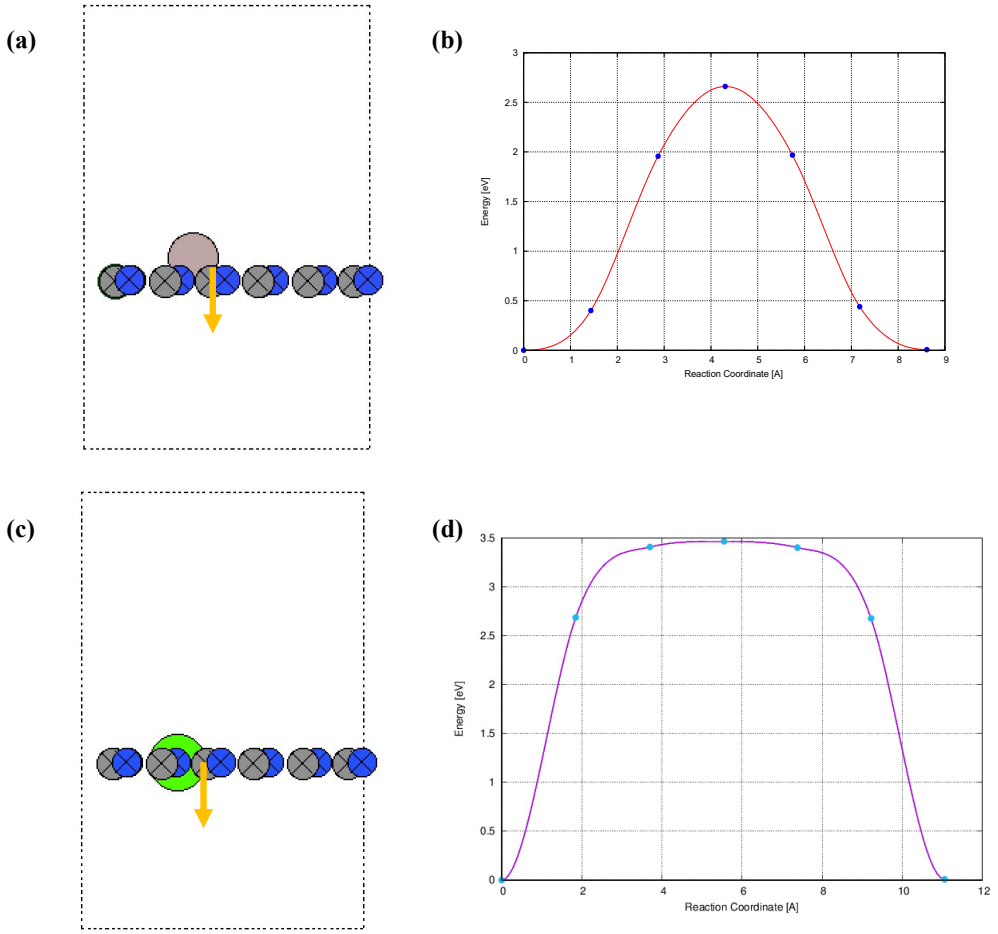

Figure 8. (**a**) The migration of one Al atom within one pore of g-C_3N_4 monolayer; (**b**) the minimum energy path of the escape mechanism of one Al atom from the pore; (**c**) The migration of one Mg atom within one pore of g-C_3N_4 monolayer; (**d**) the minimum energy path of the escape mechanism of one Mg atom from the pore.

To accurately determine the escape barrier of an Al atom within g-C_3N_4 monolayer (the energy barrier for single Al atom to move from one pore to another), the climbing image-nudged elastic band (CI-NEB) method [52] was employed, the convergence criterion of electron step is set to 10^{-6} eV. As can seen in the figure below, the estimated escape barrier is 2.66 eV, indicating that the Al atom migration between pores is prohibitively unfavorable at 300 K.

3.2. Hydrogen Storage by Al-Decorated g-C_3N_4

After elucidating the binding structure of the Al-decorated g-C_3N_4, and its stability, we now evaluate its H_2 storage capabilities. The optimized configurations are summarized in Figure 9. To determine the adsorption motif, we first consider the electronic potential distribution map in Figure 10. One can see that there exist many possible adsorption sites, around Al, C and N. Then we placed hydrogen molecules around these atoms, and DFT optimizations were conducted to determine the binding stability of these configurations. It is worth noting that each Al atom transfers partial charges to g-C_3N_4, making it electropositive. Thus these Al atoms induce polarization in nearby hydrogen molecules, enhancing the binding interaction. Through the charge density difference and PDOS (shown in Figures 11 and 12), we see that within the polarized hydrogen molecule, one H gains electrons to be electropositive and the other loses electrons to be electronegative. Thus, the electrostatic attraction between Al and these polarized hydrogen molecules can be attributed to a dipole-charge interaction. Though the electrostatic interaction is dominant for the adsorption, the van der Waals interaction also plays an important role [48]. And it is worth noting that the calculations conducted in this study are focused on physical adsorption investigation, instead of chemical reactivity analysis.The binding energy of a single H_2 on Al is around 0.26 eV; such a value is comparable to that on Mg-decorated g-C_3N_4 (0.23 eV) [37].

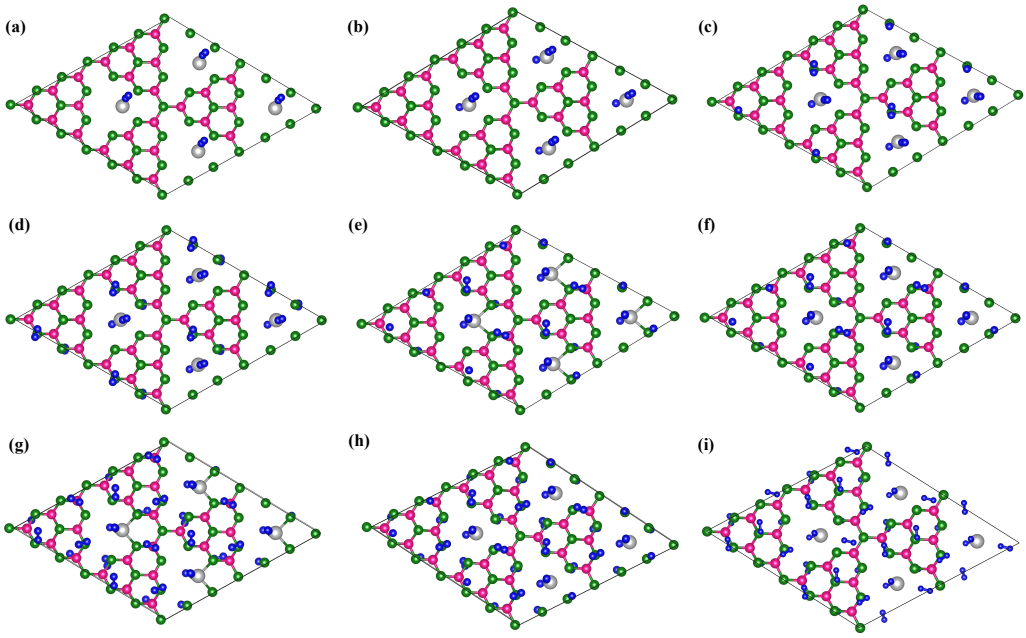

Figure 9. (**a**–**i**) The optimized configurations of the Al-decorated g-C_3N_4 with adsorbed H_2 molecules.

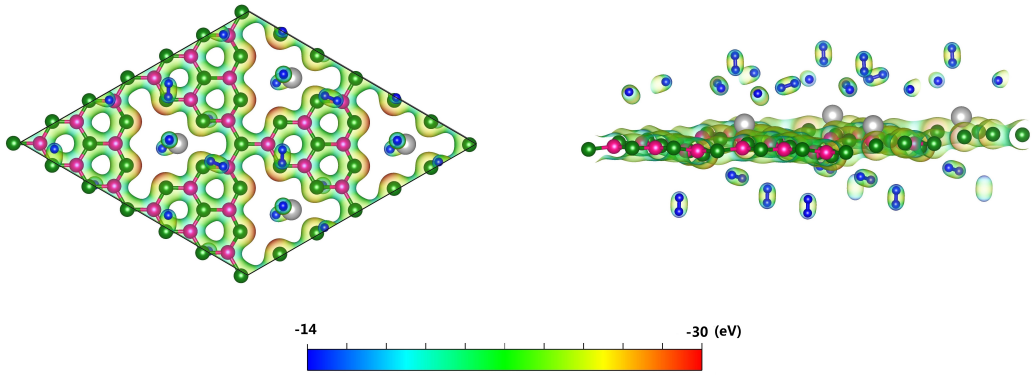

Figure 10. The map of electrostatic potential distribution for the Al−decorated g-C_3N_4 with adsorbed H_2 molecules.

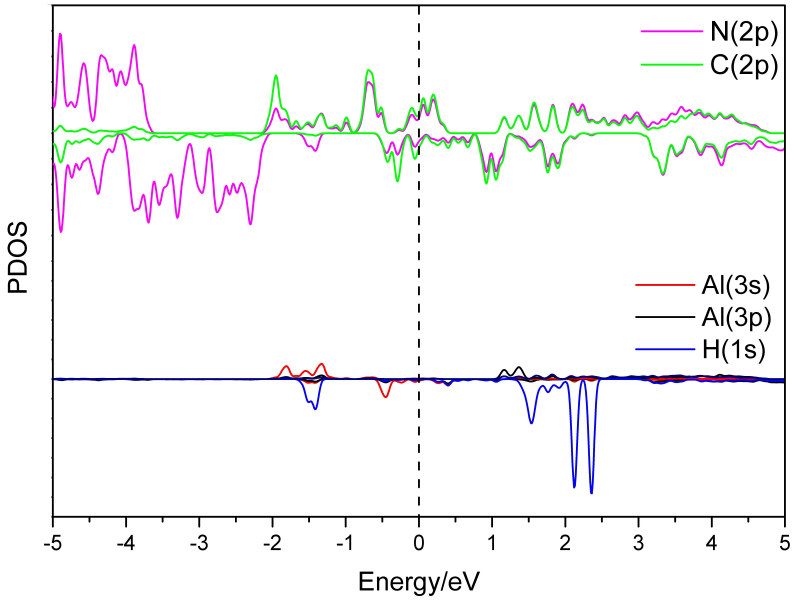

Figure 11. The PDOS of Al-decorated g-C_3N_4 with adsorbed H_2 molecules, shown for selected N, C, Al and H atoms. The energy was plotted with respect to the Fermi energy.

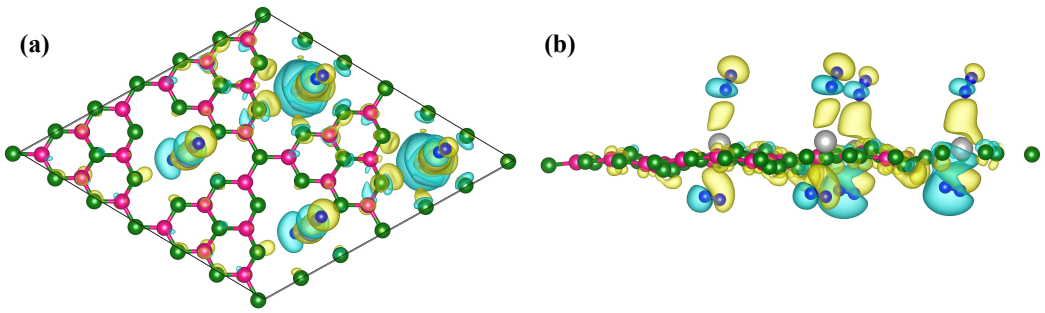

Figure 12. Charge density difference for the Al-decorated g-C_3N_4 with multiple adsorbed H_2 molecules, (**a**) top and (**b**) side view. Yellow regions indicate charge gain and blue regions indicates charge loss. The isosurface of charge density isosurface is 0.06 e/Bohr^3.

To further verify the role played by Al atom upon the adsorption ability of N atoms, we compared the H_2 binding on the pristine g-C_3N_4 with that of Al-doped g-C_3N_4. As can be seen from Figure 13, for the single H2 that was adsorbed in the vicinity of N atom of g-C_3N_4, the corresponding adsorption energy becomes much larger with the decoration of Al, indicating that Al favorably influences the material performance.

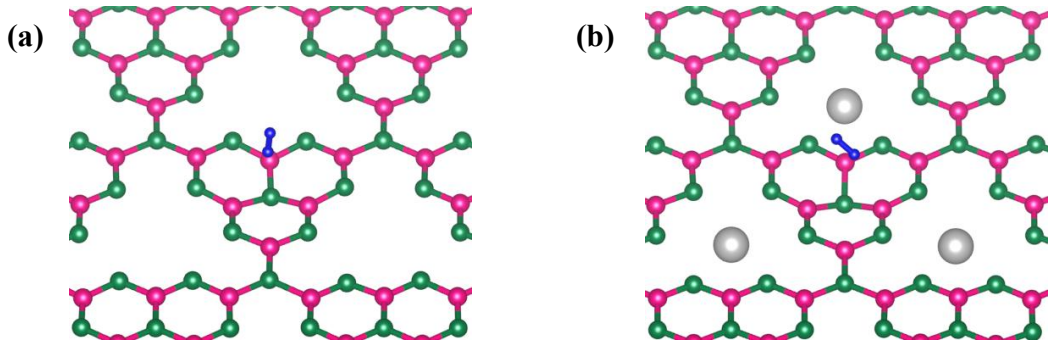

Figure 13. (**a**) The optimized configuration of the pristine g-C_3N_4 with single adsorbed H_2 molecule in the vicinity of N atom; (**b**) the optimized configuration of the Al−decorated g-C_3N_4 with single adsorbed H_2 molecule in the vicinity of N atom. The adsorption energies were presented for these two configurations.

To evaluate the adsorption capacity of hydrogen, many possible configurations were optimized, and we found that each 2 × 2 unit containing four Al atoms can adsorb at most 36 H_2 molecules. Except for the region around Al, most of the adsorbed H_2 were distributed in the vicinity of N and the C-N bonds. For these H_2 adsorbed at non-metallic sites, the molecules are bound parallel to the plane. This binding geometry can be attributed to a polarization effect, as can be seen in Figures 10 and 12, the middle region of H-H bonds tend to display electropositivity and these regions can induce a hydrogen bond like interaction with the non-metal atoms that are highly electronegative. The H_2 adsorbed by Al tend to be bound vertically. The corresponding adsorption energies, the lengths of H-H bonds, and the corresponding desorption temperatures of the optimized configurations are summarized in Table 1; we notice that all H-H bonds are stretched. It is worth noting that the adsorption energy per H_2 is negatively correlated with the total capacity of adsorption, indicating that for each possible site, there exists a maximum amount of adsorbed gas molecules.

Table 1. The adsorption energy (E_{Ads}, in eV) per H_2 on Al-decorated g-C_3N_4, the averaged H-H bonding length (in Å), the capacity of storage (wt%), and the desorption temperature (T_D, in K).

System	Adsorption E	H-H Bond	Capacity	Desorption T
$Al_4C_{24}N_{32}$ + $4H_2$	−0.26	0.760	0.94	329
$Al_4C_{24}N_{32}$ + $8H_2$	−0.14	0.758	1.86	182
$Al_4C_{24}N_{32}$ + $12H_2$	−0.13	0.756	2.76	169
$Al_4C_{24}N_{32}$ + $16H_2$	−0.13	0.756	3.65	169
$Al_4C_{24}N_{32}$ + $20H_2$	−0.11	0.754	4.52	146
$Al_4C_{24}N_{32}$ + $24H_2$	−0.11	0.754	5.38	141
$Al_4C_{24}N_{32}$ + $28H_2$	−0.11	0.753	6.22	146
$Al_4C_{24}N_{32}$ + $32H_2$	−0.10	0.753	7.05	124
$Al_4C_{24}N_{32}$ + $36H_2$	−0.10	0.753	7.86	130

4. Conclusions

The performance of Al-decorated g-C_3N_4 in hydrogen adsorption was systematically evaluated with DFT calculations; and a benchmarking study with Mg-decorated g-C_3N_4 was conducted for reference. Upon decoration of Al atoms, the semiconducting g-C_3N_4 is transformed to a conducting surface with a hydrogen storage capacity of 7.86 wt%. The Al tends to bind with N atoms, and the corresponding adsorption energy of each Al atom on g-C_3N_4 is −3.42 eV. There is partial charge transfer between the adsorbed Al and the pristine g-C_3N_4. Similar to the case of Mg-decorated g-C_3N_4, the higher electropositivity of Al facilitates polarization of the adsorbed H_2, enhancing the electrostatic interactions. A map of the electronic potential distribution was also provided in this study, and the most

possible adsorption sites, along with the corresponding adsorption energies were described. In the future, based on these initial yet fundamental investigations, we will further explore possible ways of improving the performance of metal-decorated 2D materials for clean energy gas adsorption.

Author Contributions: P.G., Z.L., J.W., and G.H. (Graeme Henkelman) designed the project. P.G. and Z.L. carried out the calculations. J.D., G.H. (Guangtong Hai), J.L., and Y.T. worked on data collection and analysis. All authors have read and agreed to the published version of the manuscript.

Funding: P.G. thanks the Australian Government that provided him an Australian International Postgraduate Award scholarship to complete his Ph.D study, during which (2017–2020) he completed this project. Work in Austin was supported by the Welch Foundation (F-1841) and the Texas Advanced Computing Center, and the National Energy Scientific Research Center. Special thanks to ByteDance Inc. for supporting calculation resources.

Data Availability Statement: The original data can be obtianed via request.

Acknowledgments: P.G. thanks the Australian Government that provided him an Australian International Postgraduate Award scholarship to complete his Ph.D study, during which (2017–2020) he completed this project. Work in Austin was supported by the Welch Foundation (F-1841) and the Texas Advanced Computing Center, and the National Energy Scientific Research Center. Special thanks to ByteDance Inc. for supporting calculation resources.

Conflicts of Interest: The authors declare no conflict of interest.

References

1. Züttel, A. Hydrogen storage methods. *Naturwissenschaften* **2004**, *91*, 157–172. [CrossRef] [PubMed]
2. Allendorf, M.D.; Hulvey, Z.; Gennett, T.; Ahmed, A.; Autrey, T.; Camp, J.; Seon Cho, E.; Furukawa, H.; Haranczyk, M.; Head-Gordon, M.; et al. An assessment of strategies for the development of solid-state adsorbents for vehicular hydrogen storage. *Energy Environ. Sci.* **2018**, *11*, 2784–2812. [CrossRef]
3. U.S. Department of Energy. *Fuel Cell Technologies Office Multi-Year Research, Development and Demonstration Plan*; U.S. Department of Energy: Washington, DC, USA, 2020.
4. Züttel, A. Materials for hydrogen storage. *Mater. Today* **2003**, *6*, 24–33. [CrossRef]
5. Huang, Z.; Autrey, T. Boron–nitrogen–hydrogen (BNH) compounds: Recent developments in hydrogen storage, applications in hydrogenation and catalysis, and new syntheses. *Energy Environ. Sci.* **2012**, *5*, 9257–9268. [CrossRef]
6. Graetz, J. New approaches to hydrogen storage. *Chem. Soc. Rev.* **2009**, *38*, 73–82. [CrossRef]
7. Bogdanović, B.; Schwickardi, M. Ti-doped alkali metal aluminium hydrides as potential novel reversible hydrogen storage materials1: Invited paper presented at the International Symposium on Metal−Hydrogen Systems. *J. Alloys Comp.* **1997**, *253–254*, 1–9.
8. Sakintuna, B.; Lamari-Darkrim, F.; Hirscher, M. Metal hydride materials for solid hydrogen storage: A review. *Int. J. Hydrogen Energy* **2007**, *32*, 1121–1140. [CrossRef]
9. Züttel, A.; Wenger, P.; Rentsch, S.; Sudan, P.; Mauron, P.; Emmenegger, C. LiBH4 a new hydrogen storage material. *J. Power Sources* **2003**, *118*, 1–7. [CrossRef]
10. Teichmann, D.; Stark, K.; Müller, K.; Zöttl, G.; Wasserscheid, P.; Arlt, W. Energy storage in residential and commercial buildings via Liquid Organic Hydrogen Carriers (LOHC). *Energy Environ. Sci.* **2012**, *5*, 9044–9054. [CrossRef]
11. Gao, P.; Huang, Z.; Yu, H. Exploration of the Dehydrogenation Pathways of Ammonia Diborane and Diammoniate of Diborane by Molecular Dynamics Simulations Using Reactive Force Fields. *J. Phys. Chem. A* **2020**, *124*, 1698–1704. [CrossRef]
12. Luo, W.; Zakharov, L.N.; Liu, S.Y. 1,2-BN Cyclohexane: Synthesis, Structure, Dynamics, and Reactivity. *J. Am. Chem. Soc.* **2011**, *133*, 13006–13009. [CrossRef]
13. Luo, W.; Campbell, P.G.; Zakharov, L.N.; Liu, S.Y. A Single-Component Liquid-Phase Hydrogen Storage Material. *J. Am. Chem. Soc.* **2011**, *133*, 19326–19329. [CrossRef]
14. Campbell, P.G.; Zakharov, L.N.; Grant, D.J.; Dixon, D.A.; Liu, S.Y. Hydrogen Storage by Boron-Nitrogen Heterocycles: A Simple Route for Spent Fuel Regeneration. *J. Am. Chem. Soc.* **2010**, *132*, 3289–3291. [CrossRef]
15. Gao, P.; Zhang, J. Understanding the Dehydrogenation Pathways of Ammonium Octahydrotriborate (NH4B3H8) by Molecular Dynamics Simulations with the Reactive Force Field (ReaxFF). *Adv. Theory Simul.* **2020**, *3*, 2000139. [CrossRef]
16. Gao, P.; Zhang, J. Understanding the Intra-Molecular Proton Transfer of Octahydrotriborate and Exploring the Dehydrogenation Pathways of NH4B3H8 by DFT Calculations. *Adv. Theory Simul.* **2021**, *4*, 2000287. [CrossRef]
17. Holst, J.R.; Gillan, E.G. From Triazines to Heptazines: Deciphering the Local Structure of Amorphous Nitrogen-Rich Carbon Nitride Materials. *J. Am. Chem. Soc.* **2008**, *130*, 7373–7379. [CrossRef]

18. Thomas, A.; Fischer, A.; Goettmann, F.; Antonietti, M.; Müller, J.O.; Schlögl, R.; Carlsson, J.M. Graphitic carbon nitride materials: variation of structure and morphology and their use as metal-free catalysts. *J. Mater. Chem.* **2008**, *18*, 4893–4908. [CrossRef]
19. Dong, G.; Zhang, Y.; Pan, Q.; Qiu, J. A fantastic graphitic carbon nitride (g-C_3N_4) material: Electronic structure, photocatalytic and photoelectronic properties. *J. Photochem. Photobiol. C Photochem. Rev.* **2014**, *20*, 33–50. [CrossRef]
20. Wei, W.; Jacob, T. Strong excitonic effects in the optical properties of graphitic carbon nitride g-C_3N_4 from first principles. *Phys. Rev. B* **2013**, *87*, 085202. [CrossRef]
21. Liu, G.; Xue, M.; Liu, Q.; Yang, H.; Zhou, Y. Facile synthesis of C-doped hollow spherical g-C_3N_4 from supramolecular self-assembly for enhanced photoredox water splitting. *Int. J. Hydrogen Energy* **2019**, *44*, 25671–25679. [CrossRef]
22. Algara-Siller, G.; Severin, N.; Chong, S.Y.; Björkman, T.; Palgrave, R.G.; Laybourn, A.; Antonietti, M.; Khimyak, Y.Z.; Krasheninnikov, A.V.; Rabe, J.P.; et al. Triazine-Based Graphitic Carbon Nitride: A Two-Dimensional Semiconductor. *Angew. Chem. Int. Ed. Engl.* **2014**, *53*, 7450–7455. [CrossRef] [PubMed]
23. Jürgens, B.; Irran, E.; Senker, J.; Kroll, P.; Müller, H.; Schnick, W. Melem (2,5,8-Triamino-tri-s-triazine), an Important Intermediate during Condensation of Melamine Rings to Graphitic Carbon Nitride: Synthesis, Structure Determination by X-ray Powder Diffractometry, Solid-State NMR, and Theoretical Studies. *J. Am. Chem. Soc.* **2003**, *125*, 10288–10300. [CrossRef] [PubMed]
24. Wang, G.; Zhou, F.; Yuan, B.; Xiao, S.; Kuang, A.; Zhong, M.; Dang, S.; Long, X.; Zhang, W. Strain-Tunable Visible-Light-Responsive Photocatalytic Properties of Two-Dimensional CdS/g-C_3N_4: A Hybrid Density Functional Study. *Nanomaterials* **2019**, *9*, 244. [CrossRef] [PubMed]
25. Fina, F.; Callear, S.K.; Carins, G.M.; Irvine, J.T.S. Structural Investigation of Graphitic Carbon Nitride via XRD and Neutron Diffraction. *Chem. Mater.* **2015**, *27*, 2612–2618. [CrossRef]
26. Hussain, T.; Hankel, M.; Searles, D.J. Computational Evaluation of Lithium-Functionalized Carbon Nitride (g-C6N5) Monolayer as an Efficient Hydrogen Storage Material. *J. Phys. Chem. C.* **2016**, *120*, 25180–25188. [CrossRef]
27. Gao, P.; Li, J.; Wang, G. Computational evaluation of superalkali-decorated graphene nanoribbon as advanced hydrogen storage materials. *Int. J. Hydrogen Energy* **2021**, *46*, 24510–24516. [CrossRef]
28. Liu, A.Y.; Cohen, M.L. Prediction of New Low Compressibility Solids. *Science* **1989**, *245*, 841–842. [CrossRef]
29. Zhu, G.; Lü, K.; Sun, Q.; Kawazoe, Y.; Jena, P. Lithium-doped triazine-based graphitic C3N4 sheet for hydrogen storage at ambient temperature. *Comput. Mater. Sci.* **2014**, *81*, 275–279. [CrossRef]
30. Nair, A.A.; Sundara, R.; Anitha, N. Hydrogen storage performance of palladium nanoparticles decorated graphitic carbon nitride. *Int. J. Hydrogen Energy* **2015**, *40*, 3259–3267. [CrossRef]
31. Panigrahi, P.; Kumar, A.; Karton, A.; Ahuja, R.; Hussain, T. Remarkable improvement in hydrogen storage capacities of two-dimensional carbon nitride (g-C_3N_4) nanosheets under selected transition metal doping. *Int. J. Hydrogen Energy* **2020**, *45*, 3035–3045. [CrossRef]
32. Zhang, Y.; Sun, H.; Chen, C. New template for metal decoration and hydrogen adsorption on graphene-like C3N4. *Phys. Lett. A* **2009**, *373*, 2778–2781. [CrossRef]
33. Wu, M.; Wang, Q.; Sun, Q.; Jena, P. Functionalized Graphitic Carbon Nitride for Efficient Energy Storage. *J. Phys. Chem. C* **2013**, *117*, 6055–6059. [CrossRef]
34. Gao, Z.; Wang, L.; Wang, L.; Huang, J.; She, H.; Wang, Q. Construction of heterostructured g-C_3N_4@TiATA/Pt composites for efficacious photocatalytic hydrogen evolution. *Int. J. Hydrogen Energy* **2019**, *44*, 24407–24417. [CrossRef]
35. Ruan, L.; Xu, G.; Gu, L.; Li, C.; Zhu, Y.; Lu, Y. The physical properties of Li-doped g-C_3N_4 monolayer sheet investigated by the first-principles. *Mater. Res. Bull.* **2015**, *66*, 156–162. [CrossRef]
36. Wei, J.; Huang, C.; Wu, H.; Kan, E. High-capacity hydrogen storage in Li-adsorbed g-C_3N_4. *Mater. Chem. Phys.* **2016**, *180*, 440–444. [CrossRef]
37. Gao, P.; Li, J.; Zhang, J.; Wang, G. Computational exploration of magnesium-decorated carbon nitride (g-C_3N_4) monolayer as advanced energy storage materials. *Int. J. Hydrogen Energy* **2021**, *46*, 21739–21747. [CrossRef]
38. Chen, X.; Li, J.-w.; Dou, X.; Gao, P. Computational evaluation of Mg-decorated g-CN as clean energy gas storage media. *Int. J. Hydrogen Energy* **2021**, *46*, 35130–35136. [CrossRef]
39. Kresse, G.; Furthmüller, J. Efficient iterative schemes for ab initio total-energy calculations using a plane-wave basis set. *Phys. Rev. B* **1996**, *54*, 11169–11186. [CrossRef]
40. Grimme, S. Semiempirical GGA-type density functional constructed with a long-range dispersion correction. *J. Comput. Chem.* **2006**, *27*, 1787–1799. [CrossRef]
41. Perdew, J.P.; Wang, Y. Pair-distribution function and its coupling-constant average for the spin-polarized electron gas. *Phys. Rev. B* **1992**, *46*, 12947–12954. [CrossRef]
42. Perdew, J.P.; Burke, K.; Ernzerhof, M. Generalized Gradient Approximation Made Simple. *Phys. Rev. Lett.* **1996**, *77*, 3865–3868. [CrossRef] [PubMed]
43. Blöchl, P.E. Projector augmented-wave method. *Phys. Rev. B* **1994**, *50*, 17953–17979. [CrossRef] [PubMed]
44. Monkhorst, H.J.; Pack, J.D. Special points for Brillouin-zone integrations. *Phys. Rev. B* **1976**, *13*, 5188–5192. [CrossRef]
45. Chadi, D.J. Special points for Brillouin-zone integrations. *Phys. Rev. B* **1977**, *16*, 1746–1747. [CrossRef]
46. Heyd, J.; Scuseria, G.E.; Ernzerhof, M. Hybrid functionals based on a screened Coulomb potential. *J. Chem. Phys.* **2003**, *118*, 8207–8215. [CrossRef]
47. Bader, R. *Atoms in Molecules—A Quantum Theory*; Oxford University Press: Oxford, UK, 1990.

48. Gao, P.; Liu, Z.; Zhang, F. Computational Evaluation of Li-doped g-C2N Monolayer as Advanced Hydrogen Storage Media. *Int. J. Hydrogen Energy* **2022**, *47*, 3625–3632. [CrossRef]
49. Henkelman, G.; Jónsson, H. A dimer method for finding saddle points on high dimensional potential surfaces using only first derivatives. *J. Chem. Phys.* **1999**, *111*, 7010–7022. [CrossRef]
50. Henkelman, G.; Jónsson, H. Long time scale kinetic Monte Carlo simulations without lattice approximation and predefined event table. *J. Chem. Phys.* **2001**, *115*, 9657–9666. [CrossRef]
51. Xu, L.; Henkelman, G. Adaptive kinetic Monte Carlo for first-principles accelerated dynamics. *J. Chem. Phys.* **2008**, *129*, 114104. [CrossRef]
52. Henkelman, G.; Uberuaga, B.P.; Jónsson, H. A climbing image nudged elastic band method for finding saddle points and minimum energy paths. *J. Chem. Phys.* **2000**, *113*, 9901–9904. [CrossRef]